Geochemistry Geophysics Geosystems G3
AN ELECTRONIC JOURNAL OF THE EARTH SCIENCES
Published by AGU and the Geochemical Society

Article
Volume 10, Number 3
7 March 2009
Q03004, doi:10.1029/2008GC002280
ISSN: 1525-2027

Incorporating self-consistently calculated mineral physics into thermochemical mantle convection simulations in a 3-D spherical shell and its influence on seismic anomalies in Earth's mantle

Takashi Nakagawa
Department of Earth and Planetary Sciences, Kyushu University, Fukuoka 812-8581, Japan

Now at Institute of Geophysics, ETH Zurich, CH-8092 Zurich, Switzerland (ntakashi@ethz.ch)

Paul J. Tackley and Frederic Deschamps
Institute of Geophysics, ETH Zurich, CH-8092 Zurich, Switzerland

James A. D. Connolly
Institute of Petrology and Mineralogy, ETH Zurich, CH-8092 Zurich, Switzerland

[1] Phase assemblages of mantle rocks calculated from the ratios of five oxides (CaO-FeO-MgO-Al_2O_3-SiO_2) by free energy minimization were used to calculate the material properties density, thermal expansivity, specific heat capacity, and seismic velocity as a function of temperature, pressure, and composition, which were incorporated into a numerical thermochemical mantle convection model in a 3-D spherical shell. The advantage of using such an approach is that thermodynamic parameters are included implicitly and self-consistently, obviating the need for ad hoc parameterizations of phase transitions which can be complex in regions such as the transition zone particularly if compositional variations are taken into account. Convective planforms for isochemical and thermochemical cases are, however, not much different from those computed using our previous, simple parameterized reference state, which means that our previous results are robust in this respect. The spectrum and amplitude of seismic velocity anomalies obtained using the self-consistently calculated material properties are more "realistic" than those obtained when seismic velocity is linearly dependent on temperature and composition because elastic properties are dependent on phase relationship of mantle minerals, in other words, pressure and temperature. In all cases, the spectra are dominated by long wavelengths (spherical harmonic degree 1 to 2), similar or even longer wavelength than seismic tomographic models of Earth, which is probably due to self-consistent plate tectonics and depth-dependent viscosity. In conclusion, this combined approach of mantle convection and self-consistently calculated mineral physics is a powerful and useful technique for predicting thermal-chemical-phase structures in Earth's mantle. However, because of uncertainties in various parameters, there are still some shortcomings in the treatment of the postperovskite phase transition. Additionally, transport properties such as thermal conductivity and viscosity are not calculated by this treatment and are thus subject to the usual uncertainties.

Components: 7919 words, 10 figures, 2 tables.

Keywords: thermochemical mantle convection; spherical shell; free energy minimization; phase transitions; seismic anomalies.

Index Terms: 8124 Tectonophysics: Earth's interior: composition and state (1212, 7207, 7208, 8105); 8121 Tectonophysics: Dynamics: convection currents, and mantle plumes.

Received 14 October 2008; **Revised** 21 January 2009; **Accepted** 28 January 2009; **Published** 7 March 2009.

Nakagawa, T., P. J. Tackley, F. Deschamps, and J. A. D. Connolly (2009), Incorporating self-consistently calculated mineral physics into thermochemical mantle convection simulations in a 3-D spherical shell and its influence on seismic anomalies in Earth's mantle, *Geochem. Geophys. Geosyst.*, *10*, Q03004, doi:10.1029/2008GC002280.

1. Introduction

[2] Various high pressure and temperature experiments have been performed to determine the phase relations of major mantle mineral systems [e.g., *Irifune and Ringwood*, 1993; *Hirose*, 2002]. Especially in the upper mantle, these phase relationships are complicated because different high-pressure phase assemblages may form from the decomposition of a given low-pressure assemblage depending on temperature, pressure and bulk chemical composition. Assuming equilibrium, these realistic phase relationships can be established by finding the phase assemblage that minimizes Gibbs free energy for a given combination of oxides as a function of temperature and pressure. Recently this technique has been used by several groups [*Connolly and Kerrick*, 2002; *Stixrude and Lithgow-Bertelloni*, 2005a, 2005b; *Piazzoni et al.*, 2007; *Ricard et al.*, 2005] to reconcile seismic anomalies in the upper mantle, but it has been received less attention in the context of numerical models of whole mantle convection, which are the subject of this work.

[3] In order to evaluate the likely form of thermal and compositional anomalies in Earth's mantle and their influence on seismic structure, numerical mantle convection simulations are required; however, phase diagrams assumed in current mantle convection simulations are very simple, so it is not clear how realistic the resulting structures are. Numerical mantle convection simulations including multiple phase transitions typically use greatly simplified phase diagrams that include only one or two transitions in the olivine system [e.g., *Tackley et al.*, 1994]. Some calculations with chemical variations have assumed a different, but still simplified, set of phase changes for the nonolivine system [*Ogawa*, 2003; *Tackley and Xie*, 2003; *Xie and Tackley*, 2004a, 2004b; *Nakagawa and Tackley*, 2005a, 2005b]. The advantage of incorporating more realistic phase relations, such as those computed by free energy minimization, is the inclusion of realistic variation of thermodynamic parameters such as density, specific heat capacity, thermal expansivity and elastic properties, which are dependent on mineralogy. Here we calculate, as a function of temperature and pressure, mineral assemblages and the resulting thermodynamic properties for compositions given as the ratio of five oxides (CFMAS (CaO-FeO-MgO-Al_2O_3-SiO_2)), using the Perple_X free energy minimization program [*Connolly*, 2005], and incorporate them into a numerical mantle convection code STAGYY in a 3-D spherical shell [*Tackley*, 2008]. In this initial study, we focus on the influences of these realistic phase relationships on the convection planform and on the depth-dependent spectrum of seismic velocity anomalies, as compared to global tomographic models.

2. Model Description

2.1. Physical Properties: Overview

[4] Compositional variations are included. The mantle is assumed to consist of a mechanical mixture of two end-member materials, namely harzburgite and MORB (Mid Ocean Ridge Basalt). This is reasonable if most of the mantle has differentiated into crust and residue and has not rehomogenized at the grain scale, both of which seem likely [e.g., *Phipps Morgan*, 1998; *Gurnis and Davies*, 1986].

[5] Two alternative methods are used for calculating the variation of physical properties with temperature and pressure for the end-member compositions: a self-consistent approach using Perple_X (hereafter referred to as Perple_X properties) and the old, parameterized treatment of phase transitions and depth variation of physical properties, hereafter referred to as parameterized properties. The most important physical property is density, which is used in the momentum and continuity equations. Note that the actual three-dimensionally varying density is used in the continuity equation, not, as is common, a depth-dependent "reference state" value: this does not cause any problem with pressure waves because hydrostatic pressure (dependent on depth

Table 1. Mantle Model Physical Mantle Parameters[a]

Symbol	Meaning	Nondimensional Value	Dimensional Value
Ra_0	Rayleigh number	10^7	N/A
η_0	reference viscosity	1	1.27×10^{22}
ρ_0	reference (surface) density	1	3300 kg m^{-3}
g	gravity	1	9.8 m s^{-2}
α_0	reference (surface) thermal expansivity	1	5×10^{-5} K^{-1}
κ_0	ref. (surface) thermal difference	1	7.656×10^{-7} m^2 s^{-1}
ΔT_{sa}	temperature scale	1	2500 K
T_s	surface Temperature	0.12	300 K
L	latent heat of melting	0.2	6.25×10^5 J kg^{-1}
H	final radiogenic heating	23.2	6×10^{-12} W kg^{-1}
τ	half-life	0.00642	2.43 Ga
C_{ps}	reference heat capacity	1	1250 J K/mol

[a] $Ra_0 = \rho_0 g \alpha_0 \Delta T_{sa} d^3 / \kappa_0 \eta_0$. For radioactive heating, the value is averaged over the whole mantle because basaltic material has 10 times higher internal heating than harzburgitic material.

only) is used to calculate density, not total pressure. In the energy equation, the key phase change related physical properties are effective thermal expansivity and effective heat capacity. These are called "effective" because they include the effects of latent heat release or absorption [see *Christensen and Yuen*, 1985] and may therefore differ from conventional thermodynamic definitions. Transport properties are not calculated by Perple_X. In both treatments the thermal diffusivity is specified as a power law dependence on density while viscosity is specified later.

[6] With the assumption of the truncated anelastic approximation, the nondimensional energy equation thus becomes:

$$\tilde{\rho}\tilde{c}_{p,eff}\left(\frac{\partial \tilde{T}}{\partial \tilde{t}} + \tilde{\mathbf{v}} \cdot \nabla \tilde{T}\right) = \nabla \cdot \left(\tilde{k} \nabla \tilde{T}\right) + \tilde{\rho}\tilde{H} - Di_0 \tilde{\alpha}_{eff} \tilde{\rho} \tilde{v}_r \tilde{T} + \frac{Di_0}{Ra_0} \tilde{\sigma}_{ij} \frac{\partial \tilde{v}_i}{\partial \tilde{x}_j} \quad (1)$$

where the tildes denote the nondimensional versions of parameters or variables, namely density ρ, effective heat capacity $c_{p,eff}$, temperature T, time t, velocity **v**, radial velocity v_r, thermal conductivity k, internal heating rate H, reference dissipation number Di_0, effective thermal expansivity α_{eff}, reference Rayleigh number Ra_0, and stress tensor σ_{ij}. These are nondimensionalized to reference values given in Table 1.

[7] The details of how density, effective heat capacity and expansivity are calculated for the two treatments are given below. In both cases, thermal diffusivity (hence conductivity) is assumed to have a power law relationship with density, i.e., thermal diffusivity $\kappa = \kappa_0(\rho_r/\rho_0)^3$ where ρ_r is the horizontally averaged reference state density and κ_0 and ρ_0 are reference values, which is based on both theoretical and experimental studies [*Anderson*, 1987; *Osako and Ito*, 1991].

2.2. Perple_X Properties

[8] The stable mineralogy and physical properties for the harzburgite and MORB lithologies were computed by free energy minimization with Perple_X [*Connolly*, 2005] as a function of pressure and temperature. For this purpose, we adopted the Mie-Grueneisen formulation of *Stixrude and Bukowinski* [1990] with the parameterization of *Stixrude and Lithgow-Bertelloni* [2005a, 2005b] augmented for lower mantle phases as described by *Khan et al.* [2006]. Here we add an adjustment on the effects of Mg postperovskite data [*Ono and Oganov*, 2005]. The parameterization limits the chemical model to the CaO-FeO-MgO-Al_2O_3-SiO_2 (CFMAS) system. For the assumed harzburgite composition (Table 2), this model is adequate to reproduce the expected lower mantle phase relations. Application of the model for the MORB composition (Table 2) is more problematic because phase equilibrium experiments [*Hirose and Fei*, 2002; *Irifune and Ringwood*, 1993; *Ono et al.*, 2005] suggest the existence of several high-pressure phases that are not characterized well enough to be included in our parameterization. Additionally, the CaO-FeO-MgO-Al_2O_3-SiO_2 model excludes volatile oxides, notably K_2O and Na_2O, which are more significant in the subducted oceanic crust, as a consequence our model is likely to overestimate the basalt-pyrolite density contrast. To calibrate this effect, we find that experimentally derived density estimates for K_2O-Na_2O-CaO-FeO-MgO-Al_2O_3-SiO_2 [*Irifune and Ringwood*, 1993; *Ono et al.*, 2005] are 1.7–2.3% below those calculated here. Accordingly, neutral buoyancy in the Earth's

Table 2. Bulk Compositions[a]

Component	Harzburgite	Pyroxenite (MORB)
SiO_2	36.04	41.75
MgO	57.14	22.42
FeO	5.41	6.00
CaO	0.44	13.59
Al_2O_3	0.96	16.24

[a] Taken from *Stixrude and Lithgow-Bertelloni* [2005b]. Unit is mol %. Pyrolite is assumed to consist of 70% harzburgite and 30% MORB composition.

interior most probably corresponds to conditions at which our basalt-pyrolite density contrast is 1.02 ± 0.03.

[9] Figure 1 shows density and S wave velocity for harzburgite and MORB compositions. The effect of the various phase transitions in the upper mantle is clearly visible, while the effect of the postperovskite transition is not clearly visible in either composition. Phase boundary slopes measured from this calculated diagram are around −3 MPa/K for the spinel → perovskite + magnesiuwüstite transition at ∼660 km depth and +12 MPa/K for the postperovskite transition. The transition pressure of postperovskite is around 125 GPa for harzburgite but slightly less for MORB, which seems to be consistent with high-pressure experiments [*Hirose*, 2006; *Ohta et al.*, 2008].

[10] As mentioned above, density is the important quantity for the momentum and continuity equations, while in the energy equation, "effective" thermal expansivity and specific heat capacity are used in order to account for latent heat effects [*Christensen and Yuen*, 1985]. Effective heat capacity $C_{P,eff}$ and effective thermal expansivity α_{eff}, for use only in the energy equation [*Gerya et al.*, 2004], are given by:

$$C_{P,eff} = \left(\frac{\partial H}{\partial T}\right)_P; \quad \alpha_{eff} = \frac{1}{T}\left[1 - \rho\left(\frac{\partial H}{\partial P}\right)_T\right] \qquad (2)$$

where H is enthalpy, T is temperature, P is pressure and ρ is density. The equation for effective expansivity is obtained through consideration of the adiabatic heating term in the energy equation, and the value differs from that calculated using the conventional definition $\alpha = \frac{1}{\rho}\left(\frac{\partial \rho}{\partial T}\right)_P$ in regions where phase transitions are supplying or absorbing latent heat. This effective thermal expansivity is never used to calculate thermal expansion, only for

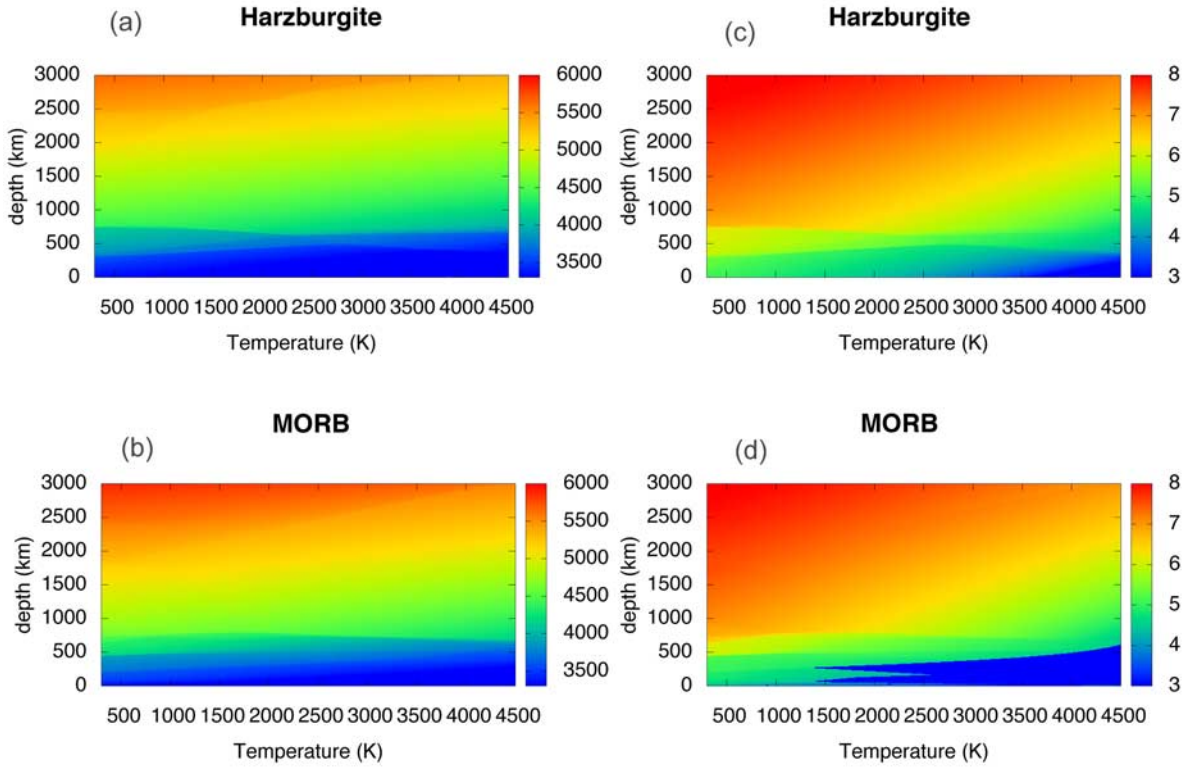

Figure 1. (a and b) Density and (c and d) shear wave velocity as a function of temperature and depth for harzburgite (Figures 1a and 1c) and MORB (Figures 1b and 1d).

heating and cooling in the energy equation. As it would be inefficient to do the free energy minimization calculation for each grid cell "on the fly" during a convection simulation the effective heat capacity and expansivity are computed from precalculated tables of ρ (P, T) and H(P, T) with a spacing of 10 km in depth and 10 K in temperature. Quantities are calculated in dimensional space then nondimensionalized for use in the code.

2.3. Parameterized Properties

[11] The "old" treatment of phase changes in StagYY is described in detail by *Tackley et al.* [2007] so is only briefly summarized here. Rocks are considered to be a mixture of "olivine" and "pyroxene/garnet," and the two systems are assumed to be independent of each other. In the olivine system, three phase changes are considered ("410," "660," postperovskite), while in the pyroxene-garnet system, four phase changes are considered (pyroxene-garnet, "410," garnet-perovskite, postperovskite). The depth of these phase changes depends on temperature. Between phase changes, physical properties vary with depth according to a reference state constructed as described by *Tackley* [1998]. The average composition is assumed to be pyrolite, which is approximated as 60% olivine and 40% pyroxene/garnet.

[12] Figure 2 compares density profiles based on this parameterized approach (Figure 2a) to those using Perple_X properties (Figure 2b). These density profiles are calculated along an adiabat with a potential temperature of 1600 K at the surface. With the parameterized approach, the density jumps due to phase transitions are very sharp, whereas with Perple_X properties, the phase transitions are fairly sharp for harzburgite but typically more spread out for MORB. In the Perple_X density profiles, a small density jump near the CMB corresponding to the postperovskite phase transition is found for harzburgite, whereas for MORB the phase change is spread out and starts at a shallower depth. The compositional density difference at the core-mantle boundary (CMB) is 2.7% between harzburgite and MORB and 2.16% between pyrolite and MORB for PERPLEX properties, but 3.6% between harzbugite and MORB and 2.32% between pyrolite and MORB for parameterized properties.

[13] Effective heat capacity and effective expansivity are given by equations similar to those introduced by *Christensen and Yuen* [1985], extended for the case of variable density and multiple phase transitions:

$$C_{p,eff} = \left(1 + Di_0 \frac{T}{\tilde{\rho}} \sum_{i=1}^{n} \overline{\gamma}_i P_i \frac{d\Gamma_i}{d\pi_i}\right); \quad \alpha_{eff} = \left(\tilde{\alpha} + \frac{1}{\tilde{\rho}} \sum_{i=1}^{n} P_i \frac{d\Gamma_i}{d\pi_i}\right) \tag{3}$$

where, for the ith phase transition, $\overline{\gamma}_i$ is the nondimensional Clapeyron slope, Pi is the phase buoyancy parameter, and the phase function Γ_i and "reduced pressure" π_i are given by

$$\Gamma_i(\pi_i) = \frac{1}{2}\left(1 + \tanh\frac{\pi_i}{d_i}\right); \quad \pi_i = z_{0i} - z - \overline{\gamma}_i(T - T_{0i}) \tag{4}$$

where (z_{0i}, T_{0i}) is a point on the phase boundary. The nondimensional Clapeyron slope and phase buoyancy parameter P are given by:

$$\overline{\gamma}_i = \frac{\gamma_i \Delta T}{\rho_i g D} \; P_i = \frac{Rb_i}{Ra} \; \overline{\gamma}_i = \frac{\gamma_i \Delta \rho_i}{\alpha \rho_i \rho_0 g D} \; \frac{Rb}{Ra} = \frac{(\Delta\rho)_i}{\alpha_0 \rho_0 \Delta T} \tag{5}$$

where ΔT is the temperature scale, D is the depth of the domain, g is the gravitational acceleration, ρ_0 is the reference density and ρ_i is the density at the depth of the ith phase transition. Note that this use of effective Cp and alpha in Stag is different from the approach used in our previous studies [e.g., *Nakagawa and Tackley*, 2004, 2005a, 2005b, 2006, 2008; *Xie and Tackley*, 2004a, 2004b; *Tackley and Xie*, 2003] of advecting potential temperature. Advecting potential temperature does not treat latent heat correctly in regions where thermal conduction is important.

2.4. Averaging Properties

[14] Composition is represented by the variable C (tracked using tracers), which varies between 0 (harzburgite) and 1 (basalt). For compositions intermediate between these end-members, a simple linear averaging of physical properties is used, except for shear wave velocity as discussed in the next section. For a generic property X, the averaged value for Perple_X properties is given by:

$$X(T, C, z) = (1 - C)X_{Harz}(T, z) + CX_{MORB}(T, z). \tag{6}$$

[15] For parameterized properties, the end-members are instead "olivine" and "pyroxene-garnet" so C is first mapped into an olivine fraction using $f_{ol} = 6/7(1 - C)$ because the initial composition of C = 0.3 everywhere is intended to represent pyrolite with

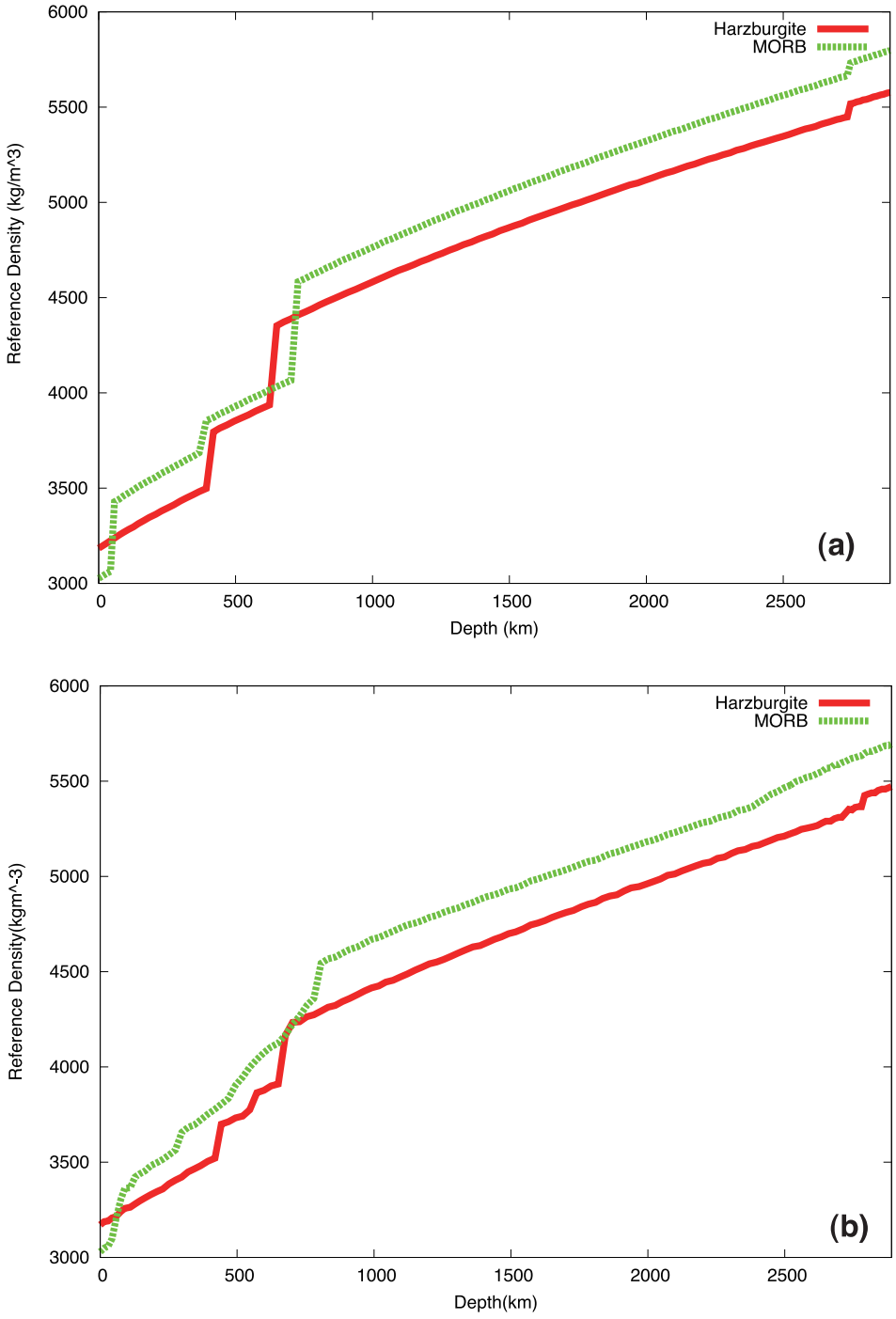

Figure 2. Density profiles along a reference adiabat with potential temperature of 1600 K at surface. (a) Linear depth-dependent properties. (b) Perple_X properties.

60% olivine and 40% pyroxene/garnet; harzburgite is (C = 0) is 6/7 olivine. Then the averaged property is calculated using:

$$X(T,C,z) = f_{ol}X_{olivine}(T,z) + (1-f_{ol})X_{px-gt}(T,z) \qquad (7)$$

2.5. Seismic Anomalies

[16] The calculation of seismic velocity anomalies makes no difference to the dynamics but is important for making comparisons to seismic observations. With Perple_X properties, elastic moduli and

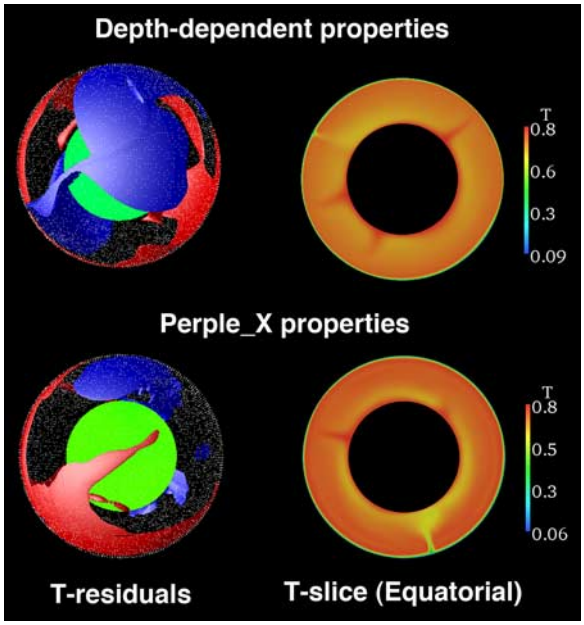

Figure 3. (left) Residual temperature isosurfaces (+250 K (red) and −250 K (blue) relative to the geotherm) and (right) equatorial slices of superadiabatic temperature for (top) the parameterized properties case and (bottom) the case with Perple_X properties.

density are calculated directly, allowing velocity to be calculated as:

$$V_s(T,C,z) = \sqrt{\frac{G(T,C,z)}{\rho(T,C,z)}} \tag{8}$$

where $G(T, C, z)$ is the phase-dependent shear modulus and $\rho(T, C, z)$ is the density. For G, Voigt-Reuss-Hill averaging is used to compute G for harzburgite and MORB lithologies from the moduli of their constituent minerals. Maps of calculated S wave velocity are shown in Figures 1c and 1d for the two end-member compositions.

[17] In the parameterized treatment, Vs anomalies are assumed to be linearly related to T and C anomalies using depth-dependent sensitivities determined from all available thermoelastic properties, including their uncertainties [*Trampert et al.*, 2001; *Deschamps and Trampert*, 2003; *Deschamps et al.*, 2007], i.e., the relationship:

$$\delta \ln V_s = \frac{\partial \ln V_s}{\partial T}\delta T + \frac{\partial \ln V_s}{\partial C}\delta C \tag{9}$$

where δT and δC are temperature and compositional anomalies relative to some radially dependent reference state. The formulae for the partial derivatives, based on fitting the curves plotted by *Deschamps and Trampert* [2003] and *Deschamps et al.* [2007] are given by:

$$\frac{\partial \ln V_s}{\partial T} = \left(-4.97 + 1.04\times 10^{-3} d - 1.08\times 10^{-8} d^2\right)\times 10^{-5}$$
$$\frac{\partial \ln V_S}{\partial C} = 0.02 \tag{10}$$

where d is the depth in kilometers. The partial derivative of Vs with respect to composition C is based on the difference between MORB and harzburgite velocities calculated using Perple_X [after *Connolly*, 2005; *Connolly and Kerrick*, 2002], which was found to be 2% faster.

2.6. Mantle Convection Simulations

[18] For mantle convection simulations, the code Stag3D, as adapted to model a spherical shell using the "Yin-Yang" grid and renamed StagYY [*Tackley*, 2008], is used. StagYY assumes the compressible truncated anelastic approximation [*Tackley*, 1996b, 1998], and can thus readily accommodate the three-dimensionally varying thermodynamics properties obtained from Perple_X. StagYY already contains the parameterized phase change treatment discussed earlier.

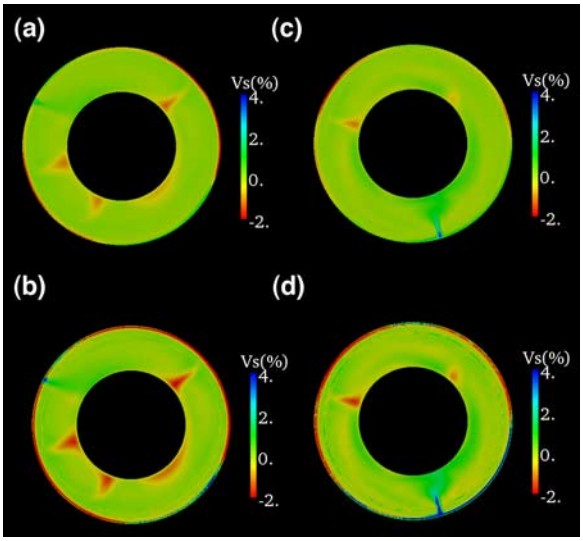

Figure 4. Equatorial slices of S wave velocity anomalies for isochemical cases. (a) Depth-dependent properties and linear scaling. (b) Depth-dependent properties and Perple_X calculated velocities. (c) Perple_X properties and linear scaling. (d) Both Perple_X properties and Perple_X scaling.

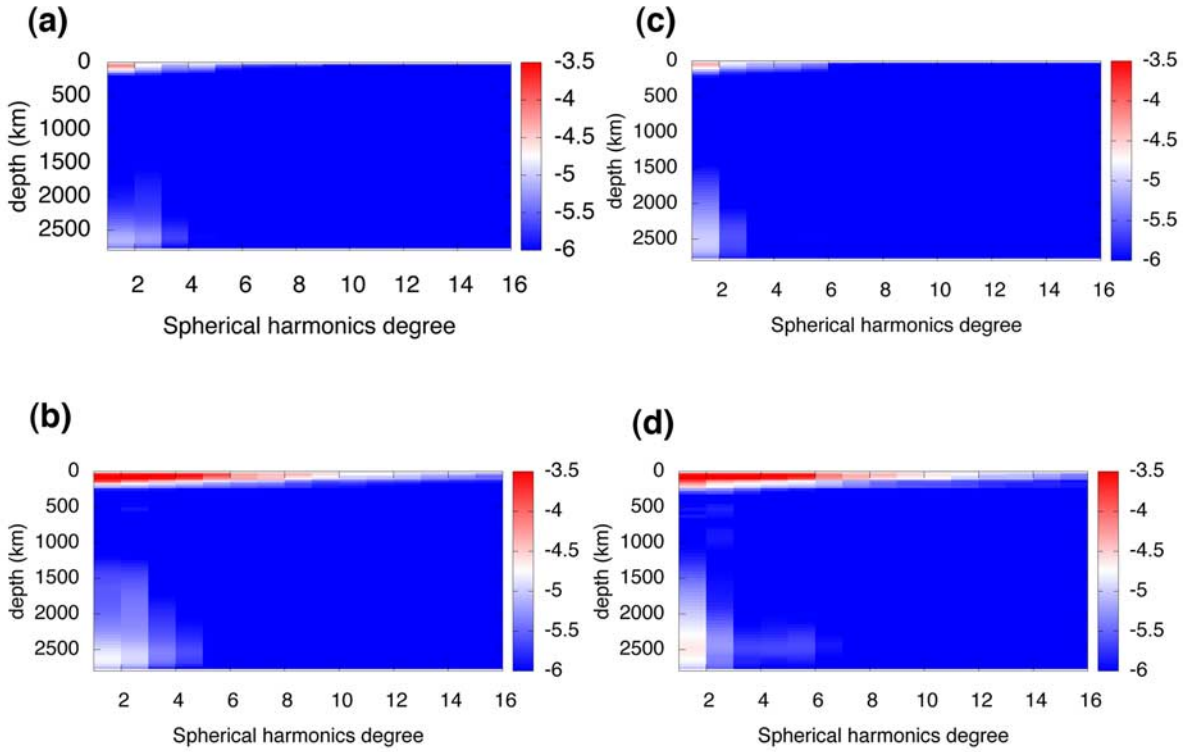

Figure 5. Spectral heterogeneity maps for isochemical cases. Color contour indicates $\log_{10}$(Power Spectra). (a) Depth-dependent properties and linear scaling. (b) Depth-dependent properties and Perple_X-calculated velocities. (c) Perple_X properties and linear scaling. (d) Both Perple_X properties and Perple_X scaling.

[19] The viscosity is assumed to depend on temperature, depth and yield stress, as given by the following nondimensional equations:

$$\eta = 2\left(\frac{1}{\eta_d} + \frac{1}{\eta_Y}\right)^{-1}$$
$$\eta_d = A_0 \exp[9.1535z] \exp\left(\frac{32.716}{T + 0.88}\right)$$
$$\eta_Y = \frac{\sigma_Y(z)}{2\dot{e}}$$
$$\sigma_Y(z) = 10^5 + 4 \times 10^5 z \qquad (11)$$

where T and z are nondimensional temperature and depth, respectively, A_0 is the viscosity prefactor that gives a nondimensional viscosity of 1 at T = 0.64 (corresponding to 1600 K dimensional temperature) and depth z = 0, and $\dot{e}$ is the second invariant of the strain rate tensor. The temperature dependence of viscosity is based on the activation energy for diffusion creep of olivine [e.g., *Karato and Wu*, 1993] and the depth dependence is adjusted to get a reasonable viscosity profile except without the usual jump at 660 km depth because viscous and plastic rheological properties are nonthermodynamic and therefore not computed by Perple_X. The yield stress at the surface is equivalent to a dimensional value of 117 MPa. Other physical properties for the simulations are also listed in Table 1.

[20] The numerical resolution used in the presented cases is 64 × 192 × 64 × 2 (equivalent to 256 points around the equator) with an average of 12 tracers per cell to track the compositional field. The initial compositional field is uniform, so compositional heterogeneities are generated from melt-induced differentiation and segregation of basaltic material from subducting slabs. The initial temperature field is an adiabat with potential temperature of 1600 K with thin boundary layers at top and bottom and random perturbations of amplitude 75 K. The core cools as heat is removed from it, according to a parameterized heat balance as discussed by *Nakagawa and Tackley* [2005a].

3. Results

[21] Four cases are shown in following subsections: (1) isochemical cases with either Perple_X properties or parameterized properties and (2) thermochemical cases with both types of properties. For the isochemical cases, the fraction of MORB is 0.3 everywhere. Each case is run for 4.5 Ga from

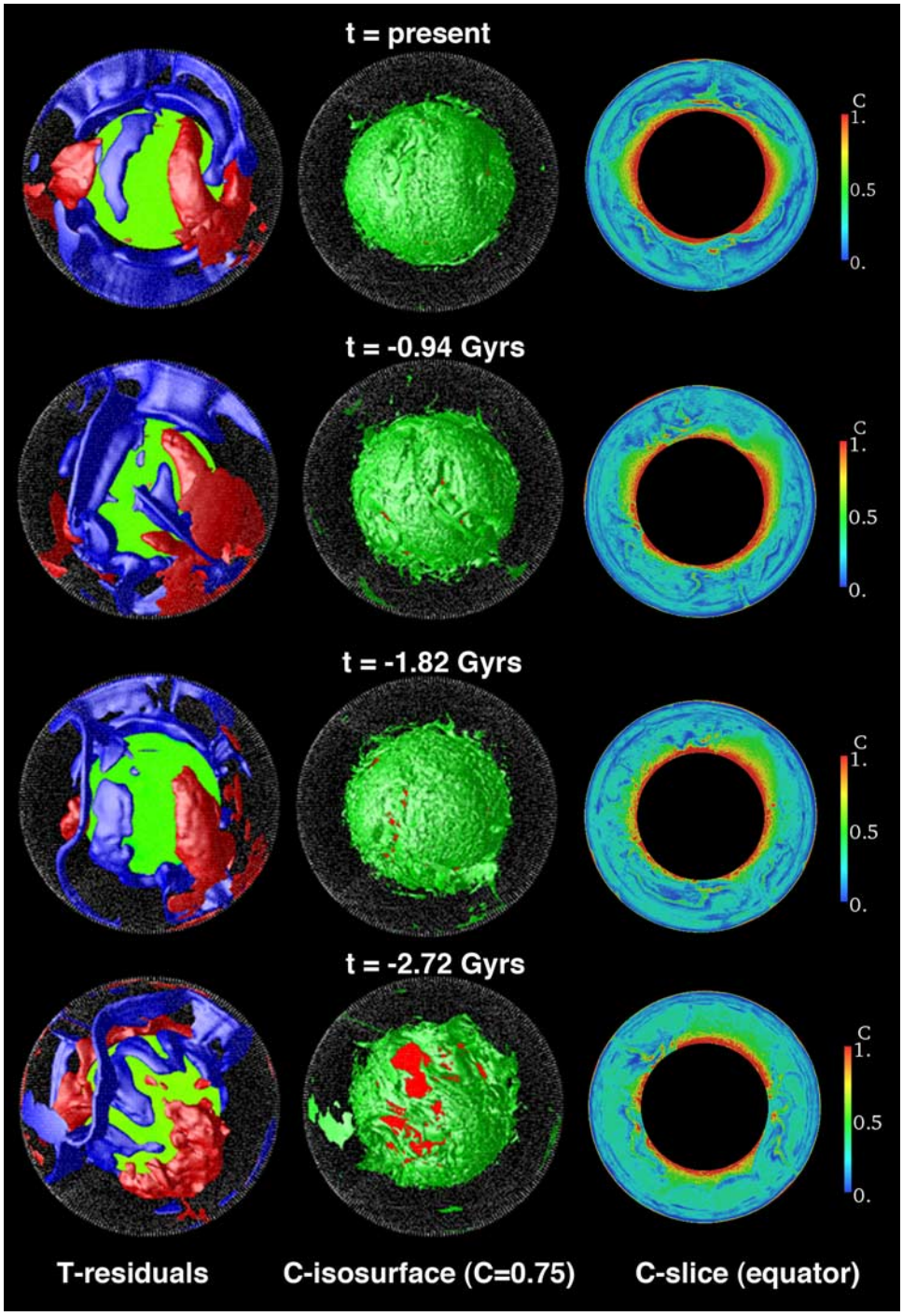

Figure 6. (left) Isosurfaces of residual temperature (−250 K (blue) and +250 K (red) relative to horizontally averaged temperature), (middle) composition isosurfaces (C = 0.75), and (right) equatorial slices of the compositional field for the thermochemical case with depth-dependent properties.

the initial state. Core cooling is assumed in all cases with an initial CMB temperature of 4390 K, which cools to ∼3500 K for isochemical cases and ∼3680 K for thermochemical cases. The computational time required for each case is ∼8–24 h using 64 CPUs of an AMD Opteron 2.2 GHz cluster at ETH Zurich. The rms. surface velocity, which is a good measure of convective vigor, is 2.43 cm/a to 3.24 cm/a for isochemical cases, but slightly slower for thermochemical cases (1.53 cm/a to 1.95 cm/a). The surface heat flow ranges from 18 TW (thermochemical cases) to 36 TW (isochemical cases), time

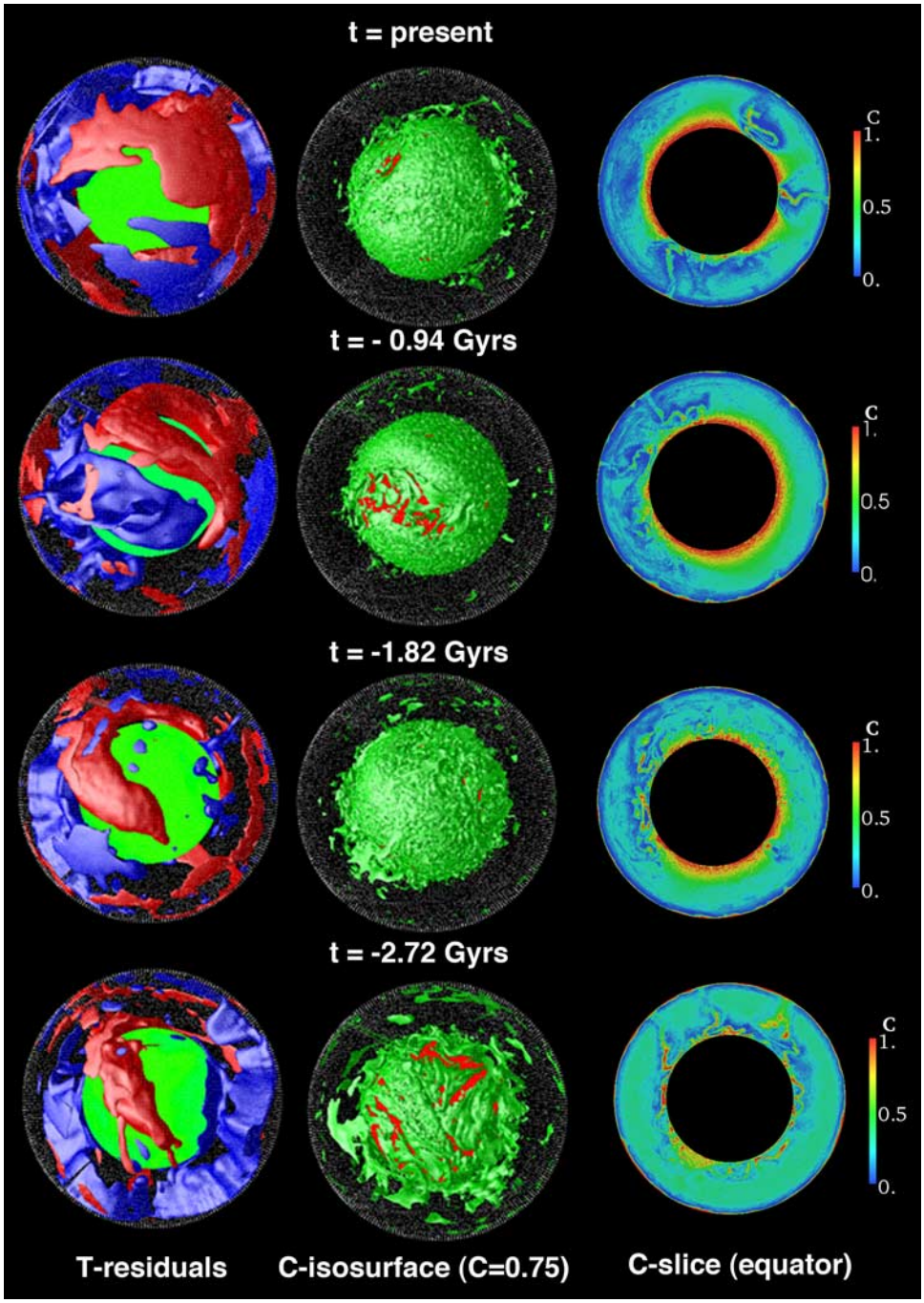

Figure 7. (left) Isosurfaces of residual temperature (−250 K (blue) and +250 K (red) relative to horizontally averaged temperature), (middle) composition isosurfaces (C = 0.75), and (right) equatorial slices of the compositional field for the thermochemical case with Perple_X properties.

averaged for 4.5 Ga. For a comparison, Earth's present-day heat loss is about 40 TW.

3.1. Isochemical Convection

[22] Figure 3 shows snapshots of temperature residuals and equatorial slices of the temperature field for the isochemical cases after 4.5 Ga of evolution. While they look broadly similar, plume activity near the core-mantle boundary displays some slight differences. This may be because of the differences (e.g., sharpness) of the postperovskite transition between the two treatments, with the sharper boundary in the parameterized properties having a stronger destabilizing effect on the

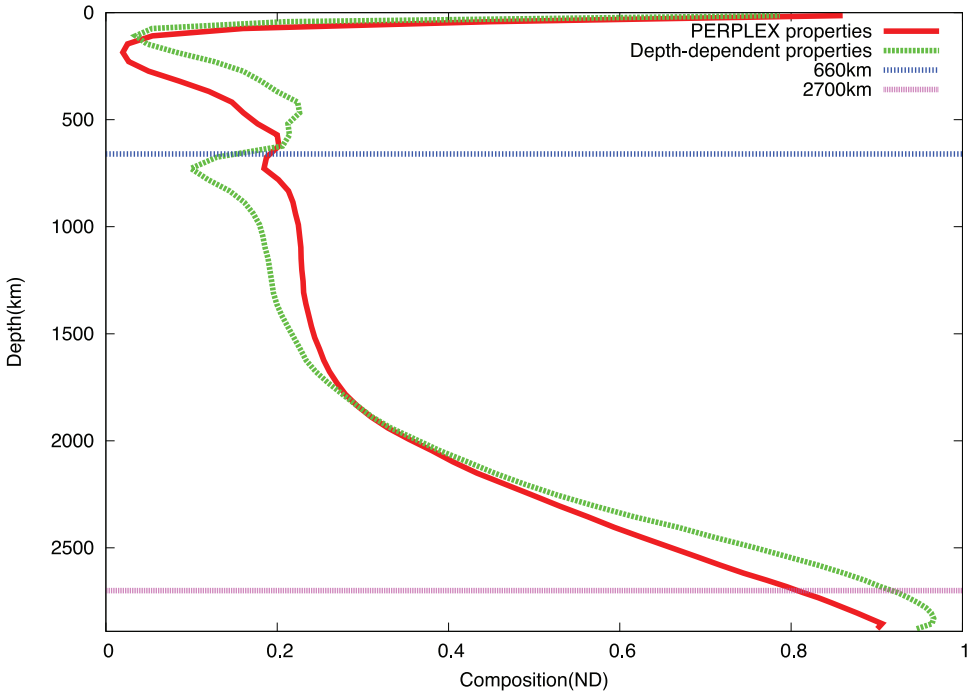

Figure 8. Radial profiles of horizontally averaged composition.

lower thermal boundary layer, and thereby promoting plume activity. Seismic anomalies reflect well the thermal structures of each case. Figure 4 shows equatorial slices of S wave anomalies for both calculations of S wave velocity. With depth-dependent scaling (Figures 4a and 4c), slow anomalies are dominant in the system while, with Perple_X-calculated Vs, anomalies are clearly visible for downwelling slabs, but upwelling plumes are less clear.

[23] Figure 5 shows spectral heterogeneity maps for each case. It is notable that the dominant heterogeneity is of very long wavelength, i.e., spherical harmonic degree 1 to 2, as would be expected from the appearance of only one long subducting slab in Figure 3. In order to isolate the effect of Vs calculation on the result, as compared to the effect of physical properties on the dynamics, each method of Vs calculation is applied for each case, a total of 4 permutations. It is clear that a stronger spectral signature in surface region is obtained for the Perple_X Vs calculation with both material property variations (Figures 5c and 5d) compared to the linear scaling approach. In the CMB region, strong heterogeneity is observed for all permutations.

3.2. Thermochemical Convection

[24] Figure 6 shows the time evolution of temperature and composition for a thermochemical case with depth-dependent properties. Dense, basaltic material covers most of the CMB by the end of the calculation. Figure 7 shows the same quantities for the equivalent case with Perple_X properties. Most features of the thermochemical structures are similar between the cases: (1) downgoing slabs penetrate into the CMB region and (2) there is a layer of

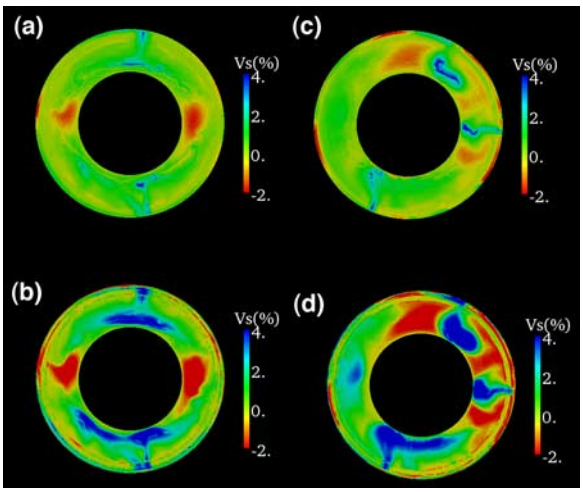

Figure 9. Equatorial slices of S wave velocity anomalies for the two thermochemical cases and two methods of calculating versus (a) depth-dependent properties and linear scaling, (b) depth-dependent properties and Perple_X velocities, (c) Perple_X properties and linear scaling, and (d) Perple_X throughout.

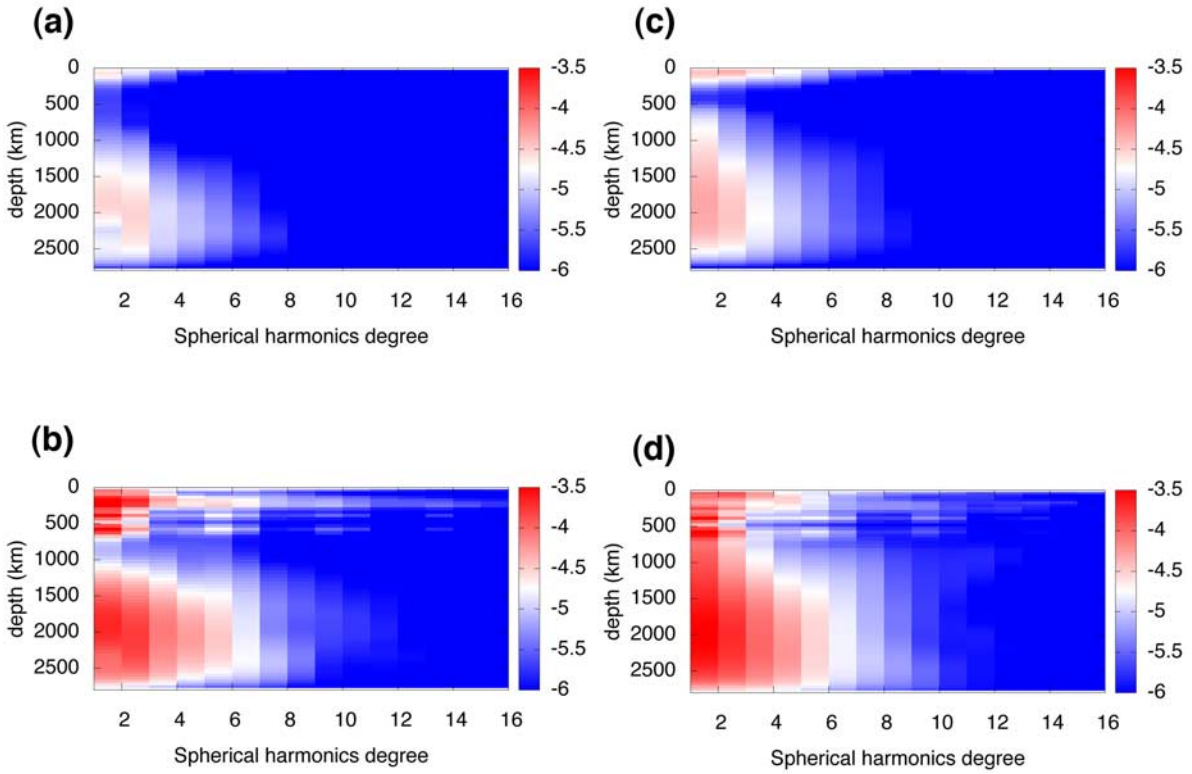

Figure 10. Spectral heterogeneity maps for the two thermochemical cases and two methods of calculating versus (a) depth-dependent properties and linear scaling, (b) depth-dependent properties and Perple_X velocities, (c) Perple_X properties and linear scaling, and (d) Perple_X throughout.

subducted MORB above the CMB that covers most of the CMB, but is pushed aside by incident downwelling slabs in a few places, exposing the core. (3) The convection is of long wavelength.

[25] Figure 8 compares azimuthally averaged radial profiles of composition for the cases with the different material property calculations. C is high (basaltic) at the top due to the crust, and at the bottom due to the buildup of segregated crust above the CMB. Around 660 km, density profiles along an adiabat (Figure 2) for the depth-dependent reference state show a density crossover between harzburgite and MORB, that is, while MORB is normally denser than harzburgite, it is less dense between ~660 km and 720 km depth. This causes pronounced compositional layering across 660 km depth, with enrichment above 660 km and depletion below 660 km. With Perple_X properties, however, this crossover barely happens, because although MORB still undergoes the transition to perovskite at greater depth, its density has already increased substantially by that point because of distributed (in depth) phase transitions occurring in the transition zone. The result of this is that the local layering around 660 km depth is much less pronounced.

[26] Figure 9 shows equatorial slices of S wave velocity anomalies for all thermochemical cases at the present time. Again, with the linear scaling between T, C and seismic wave velocity (Figures 9a and 9c), cold features are dominant, regardless of how physical properties are calculated during the simulation, whereas with the Perple_X calculated seismic wave velocity anomalies, both hot and cold features are clearly visible.

[27] Figure 10 shows spectral heterogeneity maps for thermochemical cases with both physical property calculations. As with the isochemical cases, these are dominated by long wavelengths, with spherical harmonic degree 1 to 2 being the strongest but substantial heterogeneity extending to about degree 6, which reflects the existence of only a few (and often one) long subduction zone as visible in Figures 6 and 7. There is more heterogeneity in the deep mantle than in isochemical cases because of the chemical layering that builds up there [e.g., *Tackley*, 2002]. The biggest influence on the different maps is the calculation

of seismic anomalies, rather than the physical properties used in the convection calculation. The linear scaling approach leads to stronger heterogeneity in the near-surface region, as it does for isochemical cases too. Interestingly, for the case in which everything is calculated using Perple_X, a local peak in heterogeneity is found around 660. This is also obtained from spectral profiles of several global tomography models [*Megnin and Romanowicz*, 2000; *Ritsema et al.*, 2004; *Gu et al.*, 2003]. This emphasizes the importance of using realistic phase diagrams and conversion coefficients to predict the seismological structure from mantle convection calculation.

4. Summary and Discussion

[28] The main findings of this study are as follows:

[29] 1. It is possible to incorporate the effect of realistic phase relationships based on the ratios of oxides (five oxides: CFMAS composition) into numerical thermochemical mantle convection calculations in a 3-D spherical shell. In the present study we assume all compositions to be a mixture of strips of harzburgite and MORB compositions, as would be appropriate if most of the mantle has differentiated. This obviates the necessity of introducing complicated ad hoc parameterizations of phase transitions, as the composition, temperature, and pressure dependence of geodynamically important transitions (e.g., spinel-perovskite, garnet-perovskite and perovskite-postperovskite transitions), including their phase boundaries, etc., is automatically accounted for, even at physicochemical conditions where experimental data is sparse.

[30] 2. The thermal and thermochemical structures obtained in simulations that include physical properties calculated in this way are not much different from those obtained in simulations using our old approach, in which the major phase transitions in the olivine system and pyroxene-garnet system are parameterized, and the mantle is assumed to be a mechanical mixture of these two components. This is reassuring from the perspective of previous results being robust: it is not necessary to recalculated previous cases with the new treatment. One significant difference is that the local compositional stratification around 660 km [*Ogawa*, 2003; *Nakagawa and Buffett*, 2005; *Tackley et al.*, 2005; *Xie and Tackley*, 2004a, 2004b] is less in the self-consistently calculated case, because there is a much smaller crossover of the MORB-harzburgite density relationship.

[31] 3. The seismic anomalies calculated from the self-consistent approach are significantly different from those calculated assuming a linear scaling between δVs, T and C. Specifically, heterogeneity in the near-surface region is strengthened with Perple_X properties because, in the upper mantle, there are many phase transitions thus the complicated phase relationship is reflected in complicated shear wave velocity profiles. Looking at spectral profiles near 660 km depth and near the CMB, the anomalies calculated using Perple_X for both shear velocity and other physical properties are somewhat more promising for understanding heterogeneous structures obtained by global tomography models. However, our obtained seismic images and spectral heterogeneity maps (SHMs) are not very similar to those evaluated from global tomography models [e.g., *Becker and Boschi*, 2002]. Points that could improve this are discussed below. One potentially important influence on seismic velocities is anelasticity. *Matas and Bukowinski* [2007] find that anelasticity can make a difference of 20% in the velocity temperature derivatives at 2600 km depth. While this is less than the $\sim$40–50% difference in derivatives between the two approaches tested here, it is clearly still significant.

[32] 4. All cases display very long wavelength heterogeneity consistent with, or even longer wavelength than, seismic tomographic models of Earth's mantle. This is interesting because simple convection models display heterogeneity that is too short wavelength: thus many studies have sought to explain why Earth's heterogeneity is long wavelength. Proposed explanations that are self-consistent (i.e., not imposing any geometry at the surface) include a viscosity increasing gradually with depth [*Hansen et al.*, 1993] or at 660 km [*Bunge et al.*, 1996; *Tackley*, 1996a], a low-viscosity layer [*McNamara and Zhong*, 2005], the action of the endothermic phase transition at 660 km depth [*Tackley et al.*, 1993, 1994; *Tackley*, 1995, 1996a], and the effect of continents [*Gurnis and Zhong*, 1991; *Yoshida et al.*, 1999; *Grigne et al.*, 2007]. In our present calculations there is only a moderate viscosity increases with depth and none at 660 km depth, and (particularly in isochemical cases) phase transitions near 660 km depth do not have a strong dynamical effect. Therefore, we hypothesize that the dominant mechanism in causing spherical harmonic degree 1 to 2 heterogeneity here is the plate tectonics–like behavior self-consistently generated by plastic yielding combined with strongly temperature-dependent viscosity [e.g., *Moresi and Solomatov*, 1998; *Tackley*, 2000], which was

recently demonstrated in 3-D spherical models to be capable of causing very long wavelength convection without any other complexity being necessary [*van Heck and Tackley*, 2008]. The latter models were, however, much simpler and of lower convective vigor than the models presented here, so it remains to be tested whether same mechanism is creating long-wavelength heterogeneity in the present calculations.

[33] Several improvements could be made in the future to improve realism. First, rheological properties (for each creep mechanism activation energy, activation volume, preexponential factor, power law exponent) should be different for each phase [e.g., *Yamazaki and Karato*, 2001], which would naturally lead to a viscosity jump at 660 km, which is thought to be dynamically important.

[34] Second, the convective vigor could be more Earth-like. While the rms. surface velocity for the isochemical cases is close to Earth-like, for the thermochemical cases it is a factor of $\sim$2 too low, as compared to the poloidal component of the rms. plate velocity. Here, the Rayleigh number defined using the upper mantle viscosity is 10^7. Increasing it to a higher value, such as 10^8, would lead to smaller-scale features that would require greater numerical resolution and take longer to run. Therefore, a possible next step is to check the effect of higher Rayleigh number in a two-dimensional geometry.

[35] Third the petrological model is very simplified, assuming that the initial material consists of 30% MORB. This is considerably larger than that assumed in other papers, such as 12.5% [*Christensen and Hoffmann*, 1994; *Brandenburg and van Keken*, 2007], and explains why our calculations produce a much thicker layer of segregated MORB above the CMB. The latter calculations also used kinematic plates, whereas we use self-consistently generated plates using a yielding rheology. In reality, pyrolite is capable of producing much more than 12.5% basalt, but the composition of the melt would change substantially by the time it got to 30% melting. A more sophisticated petrological model incorporating the effects of melting would help to resolve this issue in a self-consistent manner.

[36] Finally, the postperovskite phase transition may not be adequately represented in the Perple_X calculations, as there is still a lot of uncertainty in the parameters. In our present study, the postperovskite transition is visible in plotted density profiles such as those along an adiabat (Figure 2) for harzburgite (dominantly $MgSiO_3$) while, for the MORB composition, the calculated postperovskite phase transition is not sharp but rather spread over a depth range that starts at shallower depth than for harzburgite (Figure 2b, green line). Our current thermodynamic data for postperovskite is based on *Ono and Oganov* [2005] and *Mao et al.* [2005], and could be updated to account for more recent experimental and computational findings. In high P-T experiments, it is expected that the postperovskite phase transition exists in MORB material [*Hirose et al.*, 2005; *Hirose*, 2006], and seems to occur at shallower depth than $MgSiO_3$ [*Ohta et al.*, 2008]. However, other high-pressure experiments indicate that it would be transformed at deeper or similar pressure [*Nishio-Hamane et al.*, 2007] compared with $MgSiO_3$ because MORB contains much more alumina (Table 2). This is also inferred from first principle studies [*Tsuchiya and Tsuchiya*, 2008]. The seismic velocity of postperovskite has recently been measured using high temperature and pressure experiments [*Murakami et al.*, 2007], providing additional constraints on physical parameters.

[37] The incorporation of realistic phase relations into thermochemical mantle convection simulations demonstrates a strong connection among seismology, mineral physics and geodynamics. The may improve our geodynamic understanding of structure in the CMB region [*Lay et al.*, 2006; *van der Hilst et al.*, 2007; *Hirose*, 2006]. Several recent geodynamics modeling studies [e.g., *Ogawa*, 2003; *Nakagawa and Buffett*, 2005; *Tackley et al.*, 2005; *Xie and Tackley*, 2004a, 2004b] have pointed out the effect of the basalt density crossover below 660 km on enforcing partial compositional layering, recently termed the "basalt barrier" [*Davies*, 2008], as was predicted from mineral physics [e.g., *Irifune and Ringwood*, 1993; *Ono et al.*, 2005] and inferred from seismological data [*Cammarano and Romanowicz*, 2007; *Cobden et al.*, 2008; *Xu et al.*, 2008]. These models utilized simple parameterizations of phase transformations (Clapeyron slopes, depths, density variations etc.) whereas, in our model, phase transformations are implicit. Therefore, our model allows a self-consistent integration of geodynamics phenomena, seismological imaging and mineral physics data in both shallower regions and the deep mantle, subject to the limitations discussed earlier.

Acknowledgments

[38] We thank Taras Gerya for constructive discussions on implementing a realistic phase diagram section into mantle convection models and Boris Kaus for improving visualization on equatorial sections. Editor Peter van Keken and two anonymous reviewers gave us constructive reviews that im-

proved the manuscript. Financial support was provided by grants-in-aid (Young Scientist Category B, 20740256) by MEXT, Japan, and funding from ETH Zurich (T. N.).

References

Anderson, D. L. (1987), A seismic equation of state II. Shear properties and thermodynamics of the lower mantle, *Phys. Earth Planet. Inter.*, *45*, 307–323, doi:10.1016/0031-9201(87)90039-2.

Becker, T. W., and L. Boschi (2002), A comparison of tomographic and geodynamic mantle models, *Geochem. Geophys. Geosyst.*, *3*(1), 1003, doi:10.1029/2001GC000168.

Brandenburg, J. P., and P. E. van Keken (2007), Deep storage of oceanic crust in a vigorously convecting mantle, *J. Geophys. Res.*, *112*, B06403, doi:10.1029/2006JB004813.

Bunge, H. P., M. A. Richards, and J. R. Baumgardner (1996), Effect of depth-dependent viscosity on the planform of mantle convection, *Nature*, *379*, 436–438, doi:10.1038/379436a0.

Cammarano, F., and B. Romanowicz (2007), Insights into the nature of the transition zone from physically constrained inversion of long-period seismic data, *Proc. Natl. Acad. Sci. U. S. A.*, *104*, 9139–9144, doi:10.1073/pnas.0608075104.

Christensen, U. R., and A. W. Hoffmann (1994), Segregation of subducted oceanic crust in the convecting mantle, *J. Geophys. Res.*, *99*, 19,867–19,884.

Christensen, U. R., and D. A. Yuen (1985), Layered convection induced by phase transitions, *J. Geophys. Res.*, *90*, 10,921–10,300.

Cobden, L., S. Goes, F. Cammarano, and J. A. D. Connolly (2008), Thermochemical interpretation of one-dimensional seismic reference models for the upper mantle: Evidence for bias due to heterogeneity, *Geophys. J. Int.*, *175*, 627–648, doi:10.1111/j.1365-246X.2008.03903.x.

Connolly, J. A. D. (2005), Computation of phase equilibria by linear programming: A tool for geodynamic modeling and its application to subduction zone decarbonation, *Earth Planet. Sci. Lett.*, *236*, 524–541, doi:10.1016/j.epsl.2005.04.033.

Connolly, J. A. D., and D. M. Kerrick (2002), Metamorphic controls on seismic velocity of subducted oceanic crust at 100–250 km depth, *Earth Planet. Sci. Lett.*, *204*, 61–74, doi:10.1016/S0012-821X(02)00957-3.

Davies, G. F. (2008), Episodic layering of the early mantle by the basalt barrier mechanism, *Earth Planet. Sci. Lett.*, *275*, 382–392, doi:10.1016/j.epsl.2008.08.036.

Deschamps, F., and J. Trampert (2003), Mantle tomography and its relation to temperature and composition, *Phys. Earth Planet. Inter.*, *140*, 277–291, doi:10.1016/j.pepi.2003.09.004.

Deschamps, F., J. Trampert, and P. J. Tackley (2007), Thermochemical structure of the lower mantle: Seismological evidence and consequences for geodynamics, in *Superplume: Beyond Plate Tectonics*, edited by D. A. Yuen et al., pp. 293–320, Springer, New York.

Gerya, T. V., L. L. Perchuk, W. V. Maresch, and A. P. Willner (2004), Inherent gravitational instability of hot continental crust: Implications for doming and diapirism in granulite facies terrains, in *Gneiss Domes in Orogeny*, edited by D. L. Whitney, C. Teyssier, and C. S. Siddoway, *Geol. Soc. Am. Spec. Pap.*, *380*, 97–115.

Grigne, C., S. Labrosse, and P. J. Tackley (2007), Convection under a lid of finite conductivity in wide aspect ratio models: Effect of continents on the wavelength of mantle flow, *J. Geophys. Res.*, *112*, B08403, doi:10.1029/2006JB004297.

Gu, Y. J., A. M. Dziewonski, and G. Ekstrom (2003), Simultaneous inversion for mantle shear velocity and topography of transition zone discontinuities, *Geophys. J. Int.*, *154*, 559–583, doi:10.1046/j.1365-246X.2003.01967.x.

Gurnis, M., and G. F. Davies (1986), Mixing in numerical-models of mantle convection incorporating plate kinematics, *J. Geophys. Res.*, *91*, 6375–6395, doi:10.1029/JB091iB06p06375.

Gurnis, M., and S. Zhong (1991), Generation of long wavelength heterogeneity in the mantle by the dynamic interaction between plates and convection, *Geophys. Res. Lett.*, *18*, 581–584, doi:10.1029/91GL00823.

Hansen, U., D. A. Yuen, S. E. Kroening, and T. B. Larsen (1993), Dynamic consequences of depth-dependent thermal expansivity and viscosity on mantle circulations and thermal structure, *Phys. Earth Planet. Inter.*, *77*, 205–223, doi:10.1016/0031-9201(93)90099-U.

Hirose, K. (2002), Phase transitions in pyrolitic mantle around 670-km depth: Implications for upwelling of plumes from the lower mantle, *J. Geophys. Res.*, *107*(B4), 2078, doi:10.1029/2001JB000597.

Hirose, K. (2006), Postperovskite phase transition and its geophysical implication, *Rev. Geophys.*, *44*, RG3001, doi:10.1029/2005RG000186.

Hirose, K., and Y. Fei (2002), Subsolidus and melting phase relations of basaltic composition in the uppermost lower mantle, *Geochim. Cosmochim. Acta*, *66*, 2099–2108, doi:10.1016/S0016-7037(02)00847-5.

Hirose, K., N. Takafuji, N. Sata, and Y. Ohishi (2005), Phase transition and density of subducted MORB crust in the lower mantle, *Earth Planet. Sci. Lett.*, *237*, 239–251, doi:10.1016/j.epsl.2005.06.035.

Irifune, T., and A. E. Ringwood (1993), Phase transformations in subducted oceanic crust and buoyancy relationship at depths of 600–800 km in the mantle, *Earth Planet. Sci. Lett.*, *117*, 101–110, doi:10.1016/0012-821X(93)90120-X.

Karato, S., and P. Wu (1993), Rheology of the upper mantle: A synthesis, *Science*, *260*, 771–778, doi:10.1126/science.260.5109.771.

Khan, A., J. A. D. Connolly, and N. Olsen (2006), Constraining the composition and thermal state of the mantle beneath Europe from inversion of long-period electromagnetic sounding data, *J. Geophys. Res.*, *111*, B10102, doi:10.1029/2006JB004270.

Lay, T., J. Hernlund, E. J. Garnero, and M. Thorne (2006), A post-perovskite lens and D″ heat flux beneath the central Pacific, *Science*, *314*, 1272–1276, doi:10.1126/science.1133280.

Mao, W. L., et al. (2005), Iron-rich silicates in the Earth's D″ layer, *Proc. Natl. Acad. Sci. U. S. A.*, *102*, 9751–9753, doi:10.1073/pnas.0503737102.

Matas, J., and M. S. T. Bukowinski (2007), On the anelastic contribution to the temperature dependence of lower mantle seismic velocities, *Earth Planet. Sci. Lett.*, *259*, 51–65, doi:10.1016/j.epsl.2007.04.028.

McNamara, A. K., and S. Zhong (2005), Degree-one mantle convection: Dependence on internal heating and temperature-dependent rheology, *Geophys. Res. Lett.*, *32*, L01301, doi:10.1029/2004GL021082.

Megnin, C., and B. Romanowicz (2000), The three-dimensional shear velocity structure of the mantle from the inversion of body, surface and higher mode waveforms, *Geophys. J. Int.*, *143*, 709–728, doi:10.1046/j.1365-246X.2000.00298.x.

Moresi, L., and V. S. Solomatov (1998), Mantle convection with a brittle lithosphere: Thoughts on the global tectonic

styles of the Earth and Venus, *Geophys. J. Int.*, *133*, 669–682, doi:10.1046/j.1365-246X.1998.00521.x.

Murakami, M., S. V. Sinogeikin, J. D. Bass, N. Sata, Y. Ohishi, and K. Hirose (2007), Sound velocity of $MgSiO_3$ post-perovskite phase: A constraint on the D″ discontinuity, *Earth Planet. Sci. Lett.*, *259*, 18–23, doi:10.1016/j.epsl.2007.04.015.

Nakagawa, T., and B. A. Buffett (2005), Mass transport mechanism between the upper and lower mantle in numerical simulations of thermochemcial mantle convection with multicomponent phase changes, *Earth Planet. Sci. Lett.*, *230*, 11–27, doi:10.1016/j.epsl.2004.11.005.

Nakagawa, T., and P. J. Tackley (2004), Effects of thermochemical mantle convection on the thermal evolution of the Earth's core, *Earth Planet. Sci. Lett.*, *220*, 107–119, doi:10.1016/S0012-821X(04)00055-X.

Nakagawa, T., and P. J. Tackley (2005a), Deep mantle heat flow and thermal evolution of the Earth's core in thermochemical multiphase models of mantle convection, *Geochem. Geophys. Geosyst.*, *6*, Q08003, doi:10.1029/2005GC000967.

Nakagawa, T., and P. J. Tackley (2005b), The interaction between the post-perovskite phase change and a thermochemical boundary layer near the core-mantle boundary, *Earth Planet. Sci. Lett.*, *238*, 204–216, doi:10.1016/j.epsl.2005.06.048.

Nakagawa, T., and P. J. Tackley (2006), Three-dimensional structures and dynamics in the deep mantle: Effects of post-perovskite phase change and deep mantle layering, *Geophys. Res. Lett.*, *33*, L12S11, doi:10.1029/2006GL025719.

Nakagawa, T., and P. J. Tackley (2008), Lateral variations in CMB heat flux and deep mantle seismic velocity caused by a thermal-chemical-phase boundary layer in 3D spherical convection, *Earth Planet. Sci. Lett.*, *271*, 348–358, doi:10.1016/j.epsl.2008.04.013.

Nishio-Hamane, D., K. Fujino, Y. Seto, and T. Nagai (2007), Effect of the incorporation of $FeAlO_3$ into $MgSiO_3$ perovskite on the post-perovskite transition, *Geophys. Res. Lett.*, *34*, L12307, doi:10.1029/2007GL029991.

Ogawa, M. (2003), Chemical stratification in a two-dimensional convecting mantle with magmatism and moving plates, *J. Geophys. Res.*, *108*(B12), 2561, doi:10.1029/2002JB002205.

Ohta, K., K. Hirose, T. Lay, N. Sata, and Y. Ohishi (2008), Phase transitions in pyrolite and MORB at lowermost mantle conditions: Implications for a MORB-rich pile above the core-mantle boundary, *Earth Planet. Sci. Lett.*, *267*, 107–117, doi:10.1016/j.epsl.2007.11.037.

Ono, S., and A. R. Oganov (2005), In situ observations of phase transition between perobskite and CaIrO4-type phase in $MgSiO_3$ and pyrolitic mantle convection, *Earth Planet. Sci. Lett.*, *236*, 914–932, doi:10.1016/j.epsl.2005.06.001.

Ono, S., Y. Ohishi, M. Isshiki, and T. Watanuki (2005), In situ X-ray observations of phase assemblages in peridotite and basalt compositions at lower mantle conditions: Implications for density of subducted oceanic plate, *J. Geophys. Res.*, *110*, B02208, doi:10.1029/2004JB003196.

Osako, M., and E. Ito (1991), Thermal diffusivity of $MgSiO_3$ perovskite, *Geophys. Res. Lett.*, *18*, 239–242, doi:10.1029/91GL00212.

Phipps Morgan, J. (1998), Thermal and rare gas evolution of the mantle, *Chem. Geol.*, *145*, 431–445, doi:10.1016/S0009-2541(97)00153-8.

Piazzoni, A. S., G. Steinle-Neumann, H.-P. Bunge, and D. Dolejs (2007), A mineralogical model for density and elasticity of the Earth's mantle, *Geochem. Geophys. Geosyst.*, *8*, Q11010, doi:10.1029/2007GC001697.

Ricard, Y., E. Mattern, and J. Matas (2005), Synthetic tomographic images of slabs from mineral physics, in *Earth's Deep Mantle: Structure, Composition, and Evolution*, *Geophys. Monogr. Ser.*, vol. 160, edited by R. D. van der Hilst et al., pp. 283–300, AGU, Washington, D. C.

Ritsema, J., H. J. van Heist, and J. H. Woodhouse (2004), Global transition zone tomography, *J. Geophys. Res.*, *109*, B02302, doi:10.1029/2003JB002610.

Stixrude, L., and M. S. T. Bukowinski (1990), Fundamental thermodynamic relations and silicate melting with implications for the constitute of D″, *J. Geophys. Res.*, *95*, 19,311–19,325.

Stixrude, L., and C. Lithgow-Bertelloni (2005a), Thermodynamics of mantle minerals—1. Physical properties, *Geophys. J. Int.*, *162*, 610–632, doi:10.1111/j.1365-246X.2005.02642.x.

Stixrude, L., and C. Lithgow-Bertelloni (2005b), Mineralogy and elasticity of oceanic upper mantle: Origin of the low velocity zone, *J. Geophys. Res.*, *110*, B03204, doi:10.1029/2004JB002965.

Tackley, P. J. (1995), On the penetration of an endothermic phase transition by upwellings and downwelling, *J. Geophys. Res.*, *100*, 15,477–15,488, doi:10.1029/95JB00318.

Tackley, P. J. (1996a), On the ability of phase transitions and viscosity layering to induce long-wavelength heterogeneity in the mantle, *Geophys. Res. Lett.*, *23*, 1985–1988, doi:10.1029/96GL01980.

Tackley, P. J. (1996b), Effects of strongly variable viscosity on three-dimensional compressible convection in planetary mantles, *J. Geophys. Res.*, *101*, 3311–3332, doi:10.1029/95JB03211.

Tackley, P. J. (1998), Three-dimensional simulations of mantle convection with a thermochemical CMB boundary layer: D″?, in *The Core-Mantle Boundary Region*, *Geodyn. Ser.*, vol. 28, edited by M. Gurnis et al., pp. 231–253, AGU, Washington, D. C.

Tackley, P. J. (2000), Self-consistent generation of tectonic plates in time-dependent, three-dimensional mantle convection simulations, *Geochem. Geophys. Geosyst.*, *1*(8), 1021, doi:10.1029/2000GC000036.

Tackley, P. J. (2002), Strong heterogeneity caused by deep mantle layering, *Geochem. Geophys. Geosyst.*, *3*(4), 1024, doi:10.1029/2001GC000167.

Tackley, P. J. (2008), Modellng compressible mantle convection with large viscosity contrasts in a three-dimensional spherical shell using the yin-yang grid, *Phys. Earth Planet. Inter.*, *171*, 7–18.

Tackley, P. J., and S. Xie (2003), Stag3D: A code for modeling thermo-chemical multiphase convection in Earth's mantle, paper presented at Second MIT Conference on Computational Fluid and Solid Mechanics, Mass. Inst. of Technol., Cambridge, Mass.

Tackley, P. J., D. J. Stevenson, G. A. Glatzmaier, and G. Schubert (1993), Effects of an endothermic phase transition at 670 km depth in a spherical model of convection in the Earth's mantle, *Nature*, *361*, 699–704, doi:10.1038/361699a0.

Tackley, P. J., D. J. Stevenson, G. A. Glatzmaier, and G. Schubert (1994), Effects of multiple phase transitions in a three-dimensional spherical model of convection in Earth's mantle, *J. Geophys. Res.*, *99*, 15,877–15,901, doi:10.1029/94JB00853.

Tackley, P. J., S. Xie, T. Nakagawa, and J. W. Hernlund (2005), Numerical and laboratory studies of mantle convection: Philosophy, accomplishments and thermo-chemical structure evolution, in *Earth's Deep Mantle: Structure Composition, and Evolution*, *Geophys. Monogr. Ser.*, vol. 160, edited by R. D. van der Hilst et al., pp. 83–99, doi:10.1029/160GM07, AGU, Washington, D. C.

Tackley, P. J., T. Nakagawa, and J. W. Hernlund (2007), Influence of the post-perovskite transition on thermal and thermo-

chemical mantle convection, in *Post-Perovskite: The Last Phase Transition*, *Geophys. Monogr. Ser.*, vol. 174, edited by K. Hirose et al., pp. 229–247, AGU, Washington, D. C.

Trampert, J., P. Vacher, and N. Vlaar (2001), Sensitivities of seismic velocities to temperature, pressure and composition in the lower mantle, *Phys. Earth Planet. Inter.*, *124*, 255–267, doi:10.1016/S0031-9201(01)00201-1.

Tsuchiya, J., and T. Tsuchiya (2008), Postperovskite phase equilibria in the $MgSiO_3$-Al_2O_3 system, *Proc. Natl. Acad. Sci. U. S. A.*, *105*, 19,160–19,164, doi:10.1073/pnas.0805660105.

van der Hilst, R. D., M. V. de Hoop, P. Wang, and S.-H. Shim (2007), Seismostratigraphy and thermal structure of Earth's core-mantle boundary region, *Science*, *315*, 1813–1817, doi:10.1126/science.1137867.

van Heck, H., and P. J. Tackley (2008), Planforms of self-consistent generated plate tectonics in 3-D spherical geometry, *Geophys. Res. Lett.*, *35*, L19312, doi:10.1029/2008GL035190.

Xie, S., and P. J. Tackley (2004a), Evolution of helium and argon isotopes in a convecting mantle, *Phys. Earth Planet. Inter.*, *146*, 417–439, doi:10.1016/j.pepi.2004.04.003.

Xie, S., and P. J. Tackley (2004b), Evolution of U-Pb and Sm-Nd systems in numerical models of mantle convection, *J. Geophys. Res.*, *109*, B11204, doi:10.1029/2004JB003176.

Xu, W. B., C. Lithgow-Bertelloni, L. Stixrude, and J. Ritsema (2008), The effect of bulk composition and temperature on mantle seismic structure, *Earth Planet. Sci. Lett.*, *275*, 70–79, doi:10.1016/j.epsl.2008.08.012.

Yamazaki, D., and S.-I. Karato (2001), Some mineral physics constraints on the theology and geothermal structure of Earth's lower mantle, *Am. Mineral.*, *86*, 385–391.

Yoshida, M., Y. Iwase, and S. Honda (1999), Generation of plumes under a localized high viscosity lid in 3-D spherical shell convection, *Geophys. Res. Lett.*, *26*, 947–950, doi:10.1029/1999GL900147.